Laser and Particle Beams (2013), *31*, 735–745.
© Cambridge University Press, 2013 0263-0346/13 $20.00
doi:10.1017/S0263034613000785

Theoretical analysis and numerical simulation of laser driven multi-layered flyer

L. CHEN, F. WANG, AND J.Y. WU

State Key Laboratory of Explosion Science and Technology, Beijing Institute of Technology, Beijing, China

(RECEIVED 17 June 2013; ACCEPTED 20 August 2013)

Abstract

A flyer with high velocity and good integrity can be obtained by laser driven multi-layered film. In order to deeply study the action mechanism, a calculation model of laser driven multi-layered flyer has been established, taking into account the effect of multi-layered on flyer velocity increase. Multi-layered flyer velocity driven by laser pulse beam has been calculated to decide film configuration capable of forming a high velocity flyer. Taking this film configuration as object, an intense laser driven multi-layered flyer experiment has been conducted to obtain flyer velocity and verify calculation model. In order to analyze flyer motion details, a two-dimensional axisymmetric computation model of laser driven flyer has been established. In this study, laser energy spatial-temporal distribution, film ablation, and plasma absorption laser to drive flyer have been considered. Saha ionization equilibrium equation is adopted to calculate film ionization degree and give plasma state equation. Dynamic mesh algorithm is used to calculate flyer motion. Coupled numerical simulation of laser ablation, laser interaction with plasma and plasma driven flyer has been achieved. Results show that flyer velocity firstly increases and then decreases with the increase of ablation layer thickness. Ablation layer has an optical laser absorption depth for different layer materials. Plasma velocity distribution is linear in axial when flyer accelerates. Insulation layer can decrease flyer temperature effectively to keep flyer integrity.

Keywords: Flyer; Laser; Multi-layered; Numerical simulation; Plasma

INTRODUCTION

When an intense laser is focused on a metal film surface coated onto a transparent substrate, partial metal film will be ablated to produce plasma, driving the remainder to form a high velocity flyer plate, which can be used in explosive initiation and micro-space debris simulation study (Lebo *et al.*, 2008; Phipps *et al.*, 2000). In early laser driven flyer study, a single-layered film is usually employed to form the flyer plate while it has disadvantages of low laser energy absorptivity, poor flyer integrity, and a difficult increase in flyer velocity (Damian *et al.*, 2005). In the last 10 years, multi-layered film configuration is mainly adopted (Kazuo *et al.*, 2000; Kadono *et al.*, 2001), with ablation layer absorbing laser energy to produce plasma, impactor layer being driven by plasma to form a flyer plate, insulation layer holding back laser to keep flyer from being ablated and make plasma absorb more laser, resulting in a high velocity flyer plate (Paisley, 1991). Forming mechanism of plasma and detonation wave under laser loading, together with the motion law of driven flyer plate, always have been the basic issues in laser driven flyer study.

Lawrence and Trott (1991) first proposed Gurney energy calculation method of laser driven flyer velocity, in which energy conservation law was used to calculate flyer velocity, ignoring the complex interaction of laser, plasma, and flyer. Farnsworth first established one-dimensional laser driven flyer computation model, using energy deposition to simulate absorption in film (Farnworth & Lawrence, 1991). They thought only 4% of the laser energy was absorbed by film until some ionization occurs for the first part of laser pulse, and then plasma absorbed total laser energy to drive flyer motion. Cazalis *et al.* (1995) then considered plasma inverse bremsstrahlung in laser driven flyer numerical simulation. They computed plasma ionization degree, particle number, and analyzed the effects of laser power density on flyer velocity. From recent laser driven flyer studies, compared with a large amount of experimental studies (Zhao *et al.*, 2011; Dai *et al.*, 2010; Gu, 2002), theoretical calculation study is relatively weak and calculation model established is much easier, ignorance of laser energy distribution, lacking calculation

Address correspondence and reprint requests to: L. Chen, State Key Laboratory of Explosion Science and Technology, Beijing Institute of Technology, Beijing 100081, China. E-mail: chenlang@bit.edu.cn

https://doi.org/10.1017/S0263034613000785 Published online by Cambridge University Press

analysis about film phase transition under laser loading, plasma state, coupled interaction of plasma, and flyer (Farnworth & Lawrence, 1991; Cazalis *et al.*, 1995).

In this study, Gurney theory calculation method has been adopted to calculate laser driven multi-layered flyer velocity, by modifying laser energy absorption coefficient to consider the increase of laser energy deposited induced by insulation layer. The effect of film configuration on flyer velocity is analyzed, and multi-layered film configuration capable of forming a high velocity flyer plate is decided. An intense laser driven multi-layered flyer experiment has been conducted and a two-dimensional axisymmetric computation model has been established. Numerical simulation of film phase change under laser loading, plasma formation and driven flyer process has been conducted, and flyer velocity, plasma flow field characters are then analyzed.

THEORETICAL CALCULATION OF LASER DRIVEN MULTI-LAYERED FLYER VELOCITY

Calculation Method

Principle of laser driven multi-layered flyer is illustrated in Figure 1. An intense laser is focused on surface of ablation layer to ablate ablation material and produce plasma with high-temperature and high pressure. Plasma expands outward to drive both insulation layer and flyer layer as a high velocity flyer plate. Compared with single-layered film, insulation layer holds back laser energy, and flyer layer presets flyer shape, combined to keep the integrity of flyer plate.

Based on Gurney theory calculation method (Lawrence & Trott, 1991), laser driven multi-layered flyer calculation model has been established to calculate flyer maximum velocity when laser irradiates on film surface with different layer materials and configurations. A linear velocity profile assumption for plasma has been made in order to obtain flyer maximum velocity. It is finally obtained as

$$v_f = \left(\frac{3E}{\frac{3}{2}\frac{\rho_f x_f + \rho_g x_g}{\rho_b x_d} + \frac{1}{2}} \right)^{1/2}. \quad (1)$$

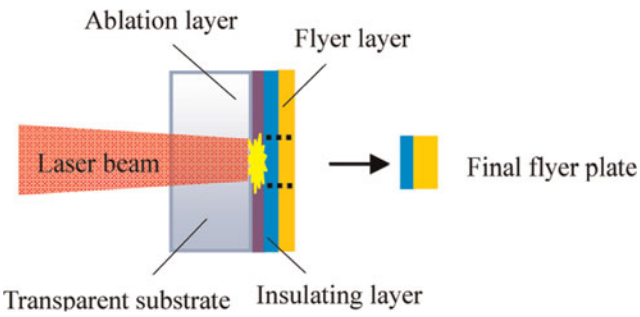


Fig. 1. (Color online) Principle of laser driven multi-layered flyer.

Where E is laser Gurney energy; ρ_b, ρ_g, ρ_f are densities of ablation layer, insulation layer, and impactor layer, respectively; x_d, x_g, x_f are ablation layer depth, insulation layer depth and impactor layer depth.

Gurney energy E can be expressed as

$$E = \frac{F_0(1-r)}{\rho_b x_d}(1 - e^{-\mu_{eff}\rho_b x_d}) - \varepsilon_d. \quad (2)$$

Where F_0 is incident laser energy density; r is laser energy loss coefficient (combing both reflective and radiative loss); ρ_b is ablation layer density; x_d is ablation depth; μ_{eff} is the effective absorption coefficient; ε_d is vaporization energy of ablation material.

Theoretical calculation has been conducted to obtain flyer maximum velocity when laser irradiates on multi-layered $Al/Al_2O_3/Al$ (250 nm/250 nm/3 μm) and $Al/Al_2O_3/Al$ (100 nm/250 nm/3 μm). Material parameters required by the model are listed in Table 1. Comparisons of flyer velocity calculated and experimental results measured by Bowden and Knowles (2009; Trott, 1994) are shown in Figure 2. Flyer maximum velocity calculated is obviously lower than experimental data, indicating that theoretical calculation model of laser driven multi-layered flyer velocity needs further revision.

For multi-layered configuration, flyer velocity can be greatly improved because of insulation layer holding back laser effectively to make ablation layer deposit more laser energy, resulting in a higher flyer velocity. Therefore, determining the effect of insulation layer on laser energy effective absorption coefficient μ_{eff} is one key issue to flyer velocity theoretical calculation. In the actual situation, as different insulation materials can be adopted, there are differences in laser energy absorbed by ablation layer. Normally experimental data is needed to determine the effect of insulation layer on μ_{eff}. In this calculation, the laser energy effective absorption coefficient μ_{eff} is modified to be $K_g \cdot \mu_{eff}$ to consider insulation layer effect. Experimental flyer velocity measured by Trott is used as a baseline to determine K_g for Al_2O_3 insulation layer (Trott, 1994). Calculation results agree well with experimental data when $K_g = 4.8$, illustrated in Figure 3. Trott's (1994) study shows that a 38% increase in flyer velocity of multi-layered flyer with Al_2O_3 insulation layer than single-layered flyer has been obtained. In this paper, flyer velocity calculated with the consideration of insulation layer effect ($K_g = 4.8$) has a 36% increase than that calculated without K_g consideration, close to Trott's experimental data of 38%, indicating the rationality of 4.8 for K_g and the validity of theoretical calculation in some extent.

Calculation Results and Analysis

Taking single film Al (3.35 μm) and multi-layered film $Al/Al_2O_3/Al$ (100 nm/250 nm/3 μm) as object, flyer velocity driven by 0–30 J/cm^2 laser energy density has been calculated. Figure 4 illustrates relation curves of calculated flyer velocities and laser fluence. Multi-layered flyer velocity is obviously higher than single-layered flyer at a laser energy

https://doi.org/10.1017/S0263034613000785 Published online by Cambridge University Press

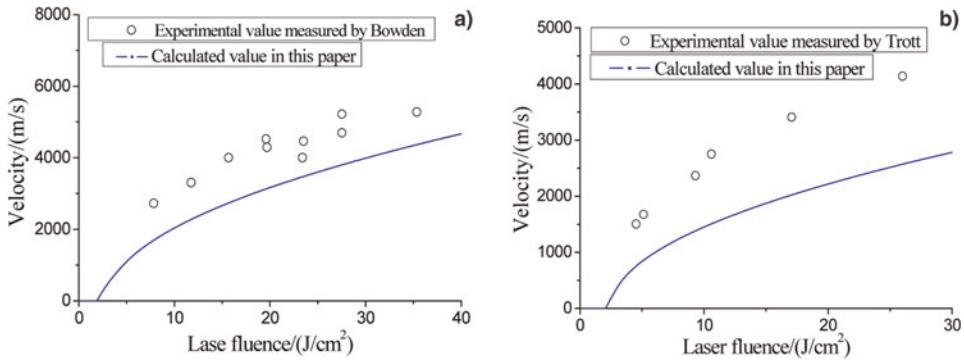


Fig. 2. (Color online) Flyer maximum velocity measured by Trott and calculated in this paper. (**a**) $Al/Al_2O_3/Al$ (250 nm/250 nm/3 μm) and (**b**) $Al/Al_2O_3/Al$ (100 nm/250 nm/3 μm).

density lower than 10 J/cm^2. The difference between multi-layered flyer velocity and single-layered flyer velocity decreases gradually as laser energy density increases. Figure 5 is relation curves of flyer velocities and laser fluence measured by Trott (1994). The trend calculated in this paper agrees well with Trott's experimental result, indicating calculation validity in some extent.

Five ablation materials of Al, Mg, Ge, C, Ti have been studied and flyer velocities have been calculated of laser irradiating on film with different ablation thicknesses. The thickness of insulation layer and impactor layer adopted in calculation are 250 nm and 3 μm, respectively. Calculation results are listed in Table 2. The data in Table 2 indicates that flyer velocity increases first and then decreases as ablation layer thickness increases for each ablation material. Ablation layer has an optical energy absorption depth. The optical energy absorption depths for Al, Mg, Ge, C, Ti at a laser fluence of 40 J/cm^2 are 350 nm, 250 nm, 200 nm, 100 nm, 100 nm, respectively. $C/Al_2O_3/Al$ (100 nm/250 nm/3 μm) has the maximum velocity of 6938.5 m/s.

LASER DRIVEN MULTI-LAYERED FLYER EXPERIMENT

Laser driven multi-layered flyer experiment has been conducted to obtain flyer velocity and verify theoretical calculation validity. Theoretical calculation results show that $C/Al_2O_3/Al$ (100 nm/250 nm/3 μm) has the maximum velocity when laser irradiates on films with different layer materials and thicknesses. Therefore, $C/Al_2O_3/Al$ (100 nm/250 nm/3 μm) has been selected as experimental research. A schematic view of the experimental set-up is given in Figure 6. Experimental system consists of solid laser, reflection/transmission mirror, focal lens, flyer generating setup, calorimeter, phototube, and oscilloscope. A high intensity solid laser pulse ($\lambda = 1064$ nm) has been divided into two beams by reflection/transmission mirror. Most of laser has been focused by an $f = 20$ cm lens onto a metal film surface in flyer generating setup to generate plasma and drive flyer. A small amount of laser has been transmitted with its energy being continuously monitored by a calorimeter. Real laser energy aiming to irradiate metal film can be computed according to energy ratio of reflection laser against transmission laser. As the action time of laser driven flyer is much shorter, it is very important to measure the start time of laser action. In the experiment, phototube has been adopted to record laser light, translating light signal into electricity signal to activate digital oscilloscope as its startup single.

Flyer generating setup is comprised of transparent substrate, multi-layered film, flat ring, and piezoelectric film target. Principle diagram of flyer generating setup is shown

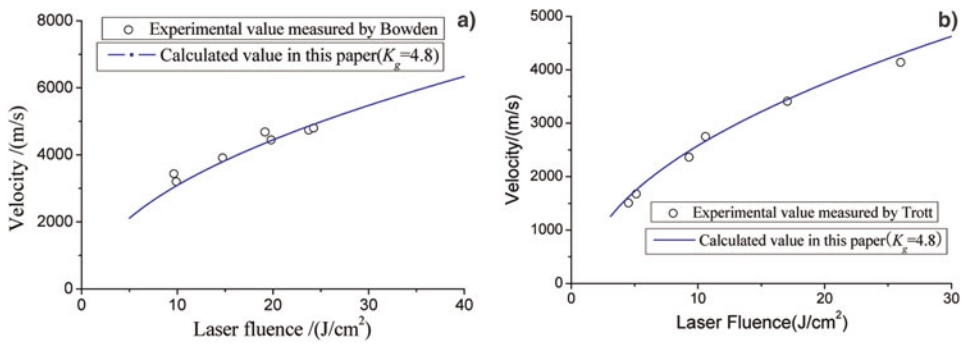


Fig. 3. (Color online) Flyer maximum velocity measured by Trott and calculated in this paper with $K_g = 4.8$. (**a**) $Al/Al_2O_3/Al$ (250 nm/250 nm/3 μm) and (**b**) $Al/Al_2O_3/Al$ (100 nm/250 nm/3 μm).

https://doi.org/10.1017/S0263034613000785 Published online by Cambridge University Press

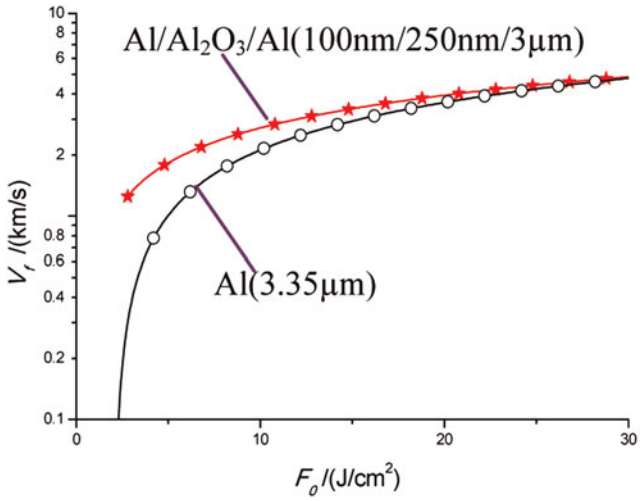


Fig. 4. (Color online) Relation curves of calculated flyer velocities.

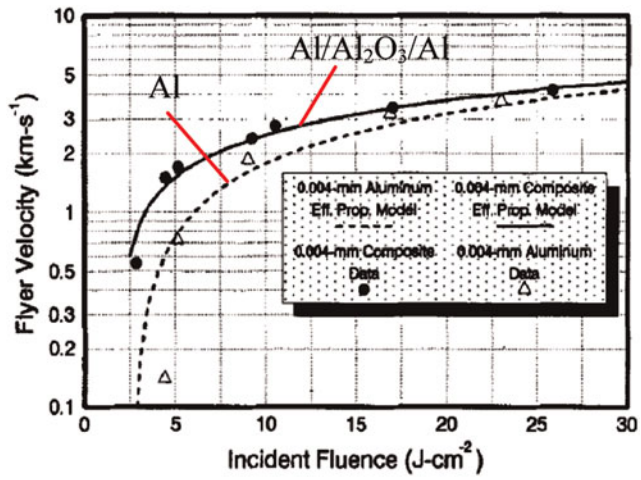


Fig. 5. (Color online) Relation curves of flyer velocities measured and laser fluence by Trott.

in Figure 7. An intense laser is focused on multi-layered surface to produce plasma and form a high velocity flyer. As flyer impacts piezoelectric film, piezoelectric signal will be recorded by digital oscilloscope (DPO 7054). According to the time difference between laser light and piezoelectric signal, the time of flyer impacting target can be determined.

Table 1. *Material parameters adopted in calculation*

Material	Density/ (g·cm)	Decomposition energy/(kJ·g^{-1})	Thermal diffusivity/ (cm^2·s^{-1})	True absorption coefficient/ (cm^2·g^{-1})
Al	2.703	12	0.96	4.4×10^5
Mg	1.74	7	0.86	1×10^5
Ti	4.54	9.85	0.09	1×10^5
Ge	5.23	5.10	0.35	1×10^5
C	2.27	59.75	0.94	1×10^5

By changing flat ring thickness, the flight time of flyer traveling different distances can be obtained. Six thicknesses of 100 μm, 150 μm, 170 μm, 200 μm, 230 μm, 250 μm for flat ring are adopted in this experiment, with a 1 μm error.

Nd: YAG solid laser has been adopted as driving laser, delivering at 1.064 μm wave length, 10 ns pulse width, and 1 J of maximum energy. The focal spot diameter is 1.1 mm. The spatial distribution of laser spot satisfies pseudo-top hat profile. Transparent substrate material is K9 glass and thickness of the transparent substrate is 3 mm. Flat ring material is polysulfone.

NUMERICAL SIMULATION OF LASER DRIVEN FLYER

In order to obtain detailed information about the laser driven flyer process, the numerical simulation work has been conducted. Laser driven flyer involves complex physical-chemical interaction in laser ablation, plasma formation, plasma expansion, film rupture, and flyer motion. It is unrealistic to describe the whole process details in simulation. Therefore, the following assumptions have been made in this paper: (1) Laser driven flyer motion is seen as two-dimensional axisymmetric motion. (2) Incident laser beam is parallel with ignorance of its focus angle. Laser energy loss is zero before it reaches film surface. (3) Film absorbs laser energy and changes from solid to vapor directly. (4) High temperature gases induced by laser ablation are in local thermodynamic equilibrium, while particle compositions follow Boltzmann distribution. Ion and electron share the same temperature. (5) Insulation and ablation layer compose the flyer plate, which is seen as rigid without deformation.

Table 2. *Flyer velocities of multi-layered flyer with different ablation thicknesses at a laser fluence of 40 J/cm^2*

Multi-layered	Flyer velocities of multi-layered flyer with different ablation depth/(m·s^{-1})							
	50 nm	100 nm	150 nm	200 nm	250 nm	300 nm	350 nm	400 nm
Mg/Al_2O_3/Al	4668.7	5682.3	6104.9	6289.9	6367.7	6394.9	6397.8	6388.9
Al/Al_2O_3/Al	4800.3	5630.7	5895.7	5969.1	5971.0	5945.3	5908.9	5868.4
Ge/Al_2O_3/Al	5524.7	6241.2	6398.1	6406.7	6373.0	6327.4	6278.7	6229.3
C/Al_2O_3/Al	6925.9	**6938.5**	6822.2	6699.9	6444.2	6405.3	6367.1	6329.6
Ti/Al_2O_3/Al	6004.9	6287.8	6263.5	6204.7	6142.1	6079.4	6017.1	5955.0

https://doi.org/10.1017/S0263034613000785 Published online by Cambridge University Press

Table 3. *Flyer maximum velocities computed and experiment data at different energies*

Laser energy/mJ	Computed flyer maximum velocity/ ($m \cdot s^{-1}$)	Experiment flyer maximum velocity/ ($m \cdot s^{-1}$)	Error/ %
300	6125	6120	0.082
210	4456	4331	2.89

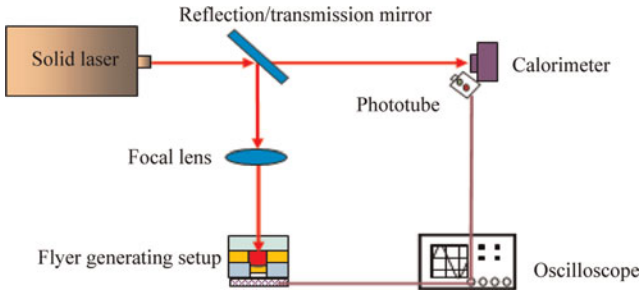


Fig. 6. (Color online) Schematic view of experimental set-up.

According to the assumptions, laser driven multi-layered flyer process can be dealt with as a fluid mechanical process. CFD numerical simulation method and Fluent 14.0 software can be adopted to conduct computation. Based on experimental setup, a two-dimensional axisymmetric computation model of laser driven multi-layered flyer has been established as shown in Figure 8. Parallel laser comes from the left side. Set the x axis as symmetry axis. Diameters of laser beam and multi-layered flyer $C/Al_2O_3/Al$ (100 nm/250 nm/3 μm) are 1 mm and 1.2 mm respectively. Computational domain is initially set at a temperature of 300 K and at a pressure of 1 atm.

Laser energy deposited in ablation layer varies with time and space. It can be expressed as (Lawrence & Trott, 1991)

$$I_L(t, r) = \frac{(1-r)\mu_{eff} F \rho}{\tau} \exp\left(-\left(\frac{t-t_0}{\tau}\right)^2\right) \times \left(1-\left(\frac{r}{w}\right)^2\right) \times \exp\left(-\int \kappa dz\right). \quad (3)$$

Where r is energy loss coefficient; μ_{eff} is effective absorption coefficient; F is laser fluence; τ is laser pulse duration; ρ is density; t_0 is the time offset of the beam maximum intensity; w is the beam radius; r and z are radial and axial coordinates, respectively; K is the plasma absorption coefficient.

Effective absorption coefficient μ_{eff} is related to true absorption coefficient, thermal diffusivity and laser pulse width. The relation is as follows (Lawrence & Trott, 1991)

$$\mu_{eff} = \frac{\mu_a}{1 + k\mu_a \rho (\sigma\tau)^{1/2}}. \quad (4)$$

Where μ_a is true absorption coefficient; ρ is density; σ is thermal diffusivity; τ is laser pulse duration; k is adjust coefficient.

The parameters to compute laser energy deposition are as follows (Bowden & Knowles, 2009): ρ is 2.27 g/cm^3, μ_a is 1.0×10^4 cm^2/g, σ is 0.94 cm^2/s, ε_d is 29.63 kJ/g, r is 0.413.

ABLATION LAYER MATERIAL PHASE TRANSITION

Ablation layer under laser loading undergoes ablation and evaporation. Gas-solid mixture model and phase transformation volume fraction have been adopted to describe ablation layer phase transition from solid to gas. Ablation layer calculation element can be seen as a mixture comprised of solid and gas. Solid volume fraction of calculation element is 1 before laser pulse, indicating no gas. During laser loading, solid ablation material transforms into gas. According to solid and gas volume fraction, film ablation and evaporation extent can be judged. The continuity, momentum and energy equations can be obtained by summing the individual continuity, momentum and energy equations for all phases. They can be expressed as

$$\frac{\partial}{\partial t}(\alpha_S \rho_S + \alpha_V \rho_V) + \nabla \cdot (\alpha_S \rho_S \vec{v} + \alpha_V \rho_V \vec{v}) = S_m, \quad (5)$$

$$\frac{\partial}{\partial t}(\rho_m \vec{v}_m) + \nabla \cdot (\rho_m \vec{v}_m \vec{v}_m) = -\nabla P + \nabla \cdot \left[\mu_m (\nabla \vec{v}_m + \nabla \vec{v}_m^T)\right] + \rho_m \vec{g} + \vec{F} + \nabla \cdot (\vec{v}_{dr} \vec{v}_{dr} \rho_m), \quad (6)$$

$$\frac{\partial}{\partial t}(\alpha_S \rho_S E_S + \alpha_V \rho_V E_V) + \nabla \cdot [\alpha_S (\rho_S E_S + P) \vec{v}_S + \alpha_V (\rho_V E_V + P) \vec{v}_V] = \nabla \cdot (k \nabla T) + S_E. \quad (7)$$

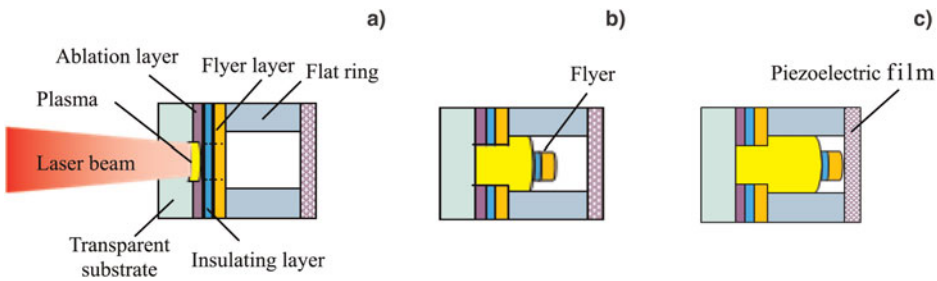


Fig. 7. (Color online) Principe diagram of flyer generating setup. (**a**) Laser induced plasma, (**b**) Flyer accelerating, (**c**) Flyer impacting target.

https://doi.org/10.1017/S0263034613000785 Published online by Cambridge University Press

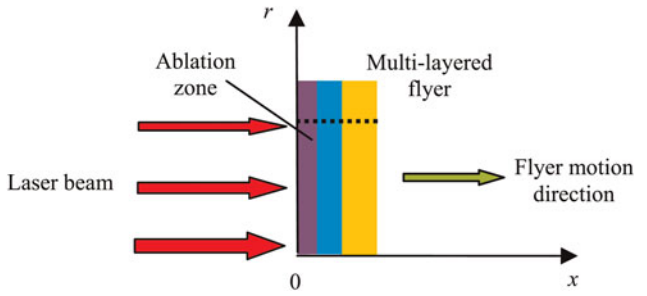


Fig. 8. (Color online) Computation model of laser driven multi-layer flyer.

In the above equations, α_S, α_V represent the volume fraction of solid phase and gas phase, respectively; ρ_S, ρ_V are solid phase density and gas phase density; $\vec{F}$ denotes a body force; $\vec{v}_{dr}$ stands for the drift velocity for vapor phase; S_m, S_E represent mass source and energy source of mixture; k denotes the thermal conductivity; ρ_m, μ_m are the mixture density and viscosity.

Two more equations define the total energy per unit mass E and enthalpy h,

$$E = h - \frac{p}{\rho} + \frac{v^2}{2},\ h_j = \int_{T_{ref}}^{T} c_{p,j} dT. \tag{8}$$

Here E, h, p, ρ, v, c_p, T represent total energy per unit mass, enthalpy, pressure, density, velocity, specific heat and temperature, respectively.

The first term on the right-hand side of energy Eq. (7) represents energy transfer due to heat conduction. The second term denotes any other volumetric heat source, including laser energy and phase transition heat. Laser energy can be obtained by summing the individual laser energy absorbed by solid and gas phase. Phase transition heat can be computed by multiplying mass transfer rate by latent heat.

$$S_E = S_L - S_{phase} = \alpha_S I_S + \alpha_V I_V - \Delta m I_m. \tag{9}$$

In the above, S_L and S_{phase} represent laser energy deposited and phase transition heat; α_S, α_V are the volume fraction of solid and gas phase; I_S, I_V stand for laser energy absorbed by solid and gas phase; Δm is mass transfer rate; I_m denote vaporization latent heat.

Based on the following temperature regimes, the mass transfer can be described as follows:

If $T > T_{sat}$

$$\dot{m}_{S\to V} = coeff * \alpha_S \rho_S \frac{T - T_{sat}}{T_{sat}}$$

If $T < T_{sat}$

$$\dot{m}_{V\to S} = coeff * \alpha_V \rho_V \frac{T_{sat} - T}{T_{sat}}$$

Where $\dot{m}_{S\to V}$ represents mass transfer rate from solid phase to gas phase; *coeff* is a relaxation time; α_S, α_V are volume fraction of solid and gas phase; ρ_S, ρ_V are solid density and gas density.

In the calculation, mass and energy transfer between solid and gas phase, together with laser energy are coupled into computation procedure via User Defined Function and solved simultaneously with the hydrodynamic system of Eqs. (5)–(7).

LASER BEAM INTERACTION WITH PLASMA

Since plasma absorbs laser energy on its way, laser intensity decays with spread of distance. It takes the following form (Moscicki *et al.*, 2011)

$$\frac{dI}{ds} = -\kappa I. \tag{10}$$

Where s is transport distance; K denotes plasma absorption coefficient, which depends on particle number and plasma temperature. The critical electron number density of plasma for laser transmission is $0.9716 \times 10^{27}/\mathrm{m}^3$ at 1.064 μm wave length.

According to Zeldovich-Raizer theory (Zeldovich & Raizer, 1980), free electron absorbs laser energy mainly through inverse Bremsstrahlung and photoionization mechanism when nanosecond laser irradiates on ablation material. Therefore, in this calculation, dominant absorption mechanisms in plasma: the electron-atom inverse Bremsstrahlung, the electron-ion inverse Bremsstrahlung and photoionization have been taken into account. Total continuous absorption coefficient (Moscicki *et al.*, 2011) can be written as

$$\kappa = \sum_{\lambda} (\kappa_{ff}^{ei}(\lambda) + \kappa_{fb}(\lambda) + \kappa_{ff}^{ea}(\lambda)) \times \left[1 - \exp\left(-\frac{hc}{\lambda k_B T}\right)\right]. \tag{11}$$

Here indices *fb* and *ff* denote free-bound and free-free transitions, and *ei* and *ea* denote electron-ion and electron-atom collisions. $K_{fb}(\lambda)$, $K_{ff}^{ei}(\lambda)$, $K_{ff}^{ea}(\lambda)$ are absorption coefficients due to photoionization, electron-ion inverse Bremsstrahlung and electron-atom inverse Bremsstrahlung, respectively. h is Planck constant; c is the speed of light in a vacuum; λ is laser wavelength; k_B is Boltzmann constant; T is plasma temperature.

$$\kappa_{fb}(\lambda) = \frac{32\pi^2 k_B}{3\sqrt{3}ch^4}\left(\frac{e_0^2}{4\pi\varepsilon_0}\right)^3 \sum_z z^2 n_{z-1} \cdot \frac{g_{z,1}}{U_{z-1}} \frac{T_e \lambda^3}{c^3} \times \exp\left(-\frac{E_j}{k_B T_e}\right)\left(\exp\left(\frac{h\upsilon}{k_B T_e}\right) - 1\right) \cdot \varepsilon(T_e, \lambda)$$

$$\kappa_{ff}^{ei}(\lambda) = \frac{8\pi e_0^6 k_B}{3m_e hc(6\pi m_e k_B)^{1/2}(4\pi\varepsilon_0)} \cdot \lambda^3 \cdot n_e T_e^{-1/2} \sum_{z=1} z^2 n_z \cdot G_{ff}$$

$$\kappa_{ff}^{ea}(\lambda) = \frac{16 e_0^2 \lambda^3}{3(4\pi\varepsilon_0) \cdot c^4 h}\left(\frac{k_B}{2\pi m_e}\right)^{3/2} n_a n_e T_e^{3/2} \times \sigma_{ea}(T) \cdot \left[1 + \left(1 + \frac{hc}{\lambda k_B T_e}\right)^2\right]. \tag{12}$$

https://doi.org/10.1017/S0263034613000785 Published online by Cambridge University Press

In the above, k_B is Boltzmann constant; h is Planck constant; c is the speed of light in a vacuum; e_0 is elementary charge; ε_0 is permittivity of vacuum; z denotes ion charge seen by free electron; n_Z and n_e are ion density and electron density, respectively; g and U stand for the statistical weight and partition function; λ and ν are laser wavelength and frequency; E is ionization energy; $\varepsilon(T_e, \lambda)$ is the Biberman factor; T_e is electron temperature; G_{ff} is the Gaunt factor; σ_{ea} is the electron-atom scattering cross-section.

PLASMA STATE EQUATION

Since gas phase of ablation layer contains a large amount of electrification particles, ideal gas state equation is not applicable any more. Therefore, plasma state equation is necessary in calculation to take into account the effect of particles number change and the coulomb force between particles on pressure and inner energy.

Plasma pressure and inner energy (Hong *et al.*, 2001) are given by

$$P = (1+\alpha)\frac{R}{M}\rho T, \tag{13}$$

$$E = \frac{3}{2}(1+\alpha)\frac{R}{M}T + N_0\sum_i \alpha_i I_i + N_0\sum_i \alpha_i \varepsilon_i. \tag{14}$$

In the above, the first term on the right-hand side represents the contribution of ion, atomic, and electron thermodynamic on inner energy. The effects of atomic ionization and excitation on inner energy are described as the second and third terms. α represents ionization degree; I_i stands for ionization energy; ε_i denotes excitation energy; N_0 is total atomic number in per unit mass.

Based on thermodynamics, the relationship between entropy, enthalpy and Helmholtz free energy is

$$S = -\left(\frac{\partial F}{\partial T}\right)_{V,N}, H = F - T\left(\frac{\partial F}{\partial T}\right)_{V,N} - V\left(\frac{\partial F}{\partial V}\right)_{T,N}, Cp = \left(\frac{\partial H}{\partial T}\right)_P. \tag{15}$$

Here F denotes Helmholtz free energy of ionized vapor.

From Eqs. (13), (14), and (15), ionization degree is a critical parameter to compute electrification vapor state equation and thermodynamic properties. As for nanosecond laser, electron collision time is only 10^{-11}s, far less than laser pulse width, and ion temperature is very close to electron temperature (Tong & Tang, 2008). Therefore, the assumption of local thermodynamic equilibrium is fulfilled, ignoring the difference between electron temperature and ion temperature. In this paper, the assumption that chemical reaction and thermodynamic behavior reach equilibrium instantaneously at the moment of laser ablation has been made to calculate plasma ionization degree. Ion and electron number can be computed by iteratively solving ionization balance equations. Then ionization degree, state equation and thermodynamic properties can be obtained.

According to Saha equation, ion and electron concentration meet the following relationship (Robert *et al.*, 2008).

$$\frac{a_i a_e}{a_{i-1}} = \frac{2}{n}\frac{u_{a^{i+}}}{u_{a^{(i-1)+}}}\left(\frac{2\pi m_e m_{a^i} + k_B}{m_{a^{(i-1)+}}h^2}\right)^{\frac{3}{2}} T^{\frac{3}{2}} \exp\left(-\frac{I_i - I_0}{k_B T}\right) = K_i(\mathrm{i} = 1, 2, 3..... \tag{16}$$

Where K_i is ionization equilibrium constant; u_a, u_a^{i+} are partition functions of atomic and ion, respectively; I_i is ionization energy; m_a, m_a^{i+} are atomic mass and ion mass; m_e is electron mass; n, n_a, n_a^{i+}, n_e are, respectively, total particle number, atomic number, ion number and electron number; a_e is ionization degree; a_0, a_i are atomic and ion concentration.

Additional conservation equations for element and charge are needed.

$$a_0 + \sum_{i=1}^{13} a_i + a_e = 1,\ a_e = \sum_{i=1}^{13} i a_i. \tag{17}$$

In Eqs. (16) and (17), there are $I+2$ unknowns and equations, forming a closed equation set. a_e can be obtained by solving the equation set. Combining a_e into Eqs. (13), (14), and (15), high temperature vapor equation of state and thermodynamic properties are computed. For ablation layer C, i is equal to 6. Since computation amount is critical huge to solve high-order nonlinear equation set, only first-order ionization reaction is considered here in order to avoid computational difficulties.

The ionization degree of first-order ionization reaction is

$$a_e = \frac{-K_1 + \sqrt{K_1^2 + 4K_1}}{2}. \tag{18}$$

Where K_1 is first order ionization equilibrium constant, which can be expressed as

$$K_1 = \frac{2}{n}\frac{u_{a^+}}{u_{a^0}}\left(\frac{2\pi m_e m_{a^{i+}} k_B}{m_{a^0}h^2}\right)^{\frac{3}{2}} T^{\frac{3}{2}} \exp\left(-\frac{I_i - I_0}{k_B T}\right).$$

In the numerical simulation, User-defined Real Gas Models is used in fluent for combining new state equation and thermodynamic properties into computation procedure, aiming at modeling plasma expansion behaviors.

FLYER MOTION

Dynamic mesh model has been employed to describe flyer motion. In numerical simulation, the flyer is seen as a rigid, and the boundary between flyer and plasma is a moving boundary. Flow field parameters adjacent to flyer

https://doi.org/10.1017/S0263034613000785 Published online by Cambridge University Press

are computed first, and then according to mechanical equilibrium, the velocity of moving boundary within time step can be computed. The grid will be regenerated and enmeshed by controlling grid volume to realize boundary moving after current location of moving boundary is obtained. The movement in next time step will be determined by current computed results.

Flyer is pushed by plasma flow field F and also subjects to resistance f in flight. Based on the theorem of momentum, flyer velocity increase Δv within Δt time can be expressed as

$$\Delta v = \frac{\overline{P} \cdot S - f}{m} \cdot \Delta t. \tag{19}$$

Where $\overline{P}$ represents average pressure of plasma flow field on flyer; S stands for action area of plasma flow field on flyer; f is resistance; m is flyer mass; Δt is time step. Resistance f includes film fraction f_{film} and air resistance f_{air}. Film friction f_{film} exists initially, and air resistance f_{air} is decided on flyer area and velocity. Both f_{film} and f_{air} is closely related to flow field thrust. Therefore, in numerical simulation, the resistance f suffered by flyer is assumed to be plasma flow field thrust F multiply by resistance coefficient k. According to flyer velocity measured in experiment at some laser energy, the resistance coefficient k can be determined. Then compare calculated flyer velocity and experiment data at other laser energy to verify the validity of numerical simulation. On this basis, plasma flow field characteristic is analyzed.

RESULTS AND DISCUSSION

Flyer Velocity Analysis

Flight time of flyers traveling different distances have been measured in experiments. The following figure is the original signals measured with the photodiode and the piezo film. The yellow line is laser signal and the green line is piezoelectric signal. The onset of laser signal is taken as time zero point, and the onset of piezoelectric signal is taken as flyer arrival time. The time difference Δt between the two onsets can be seen as flyer flight time. Based on

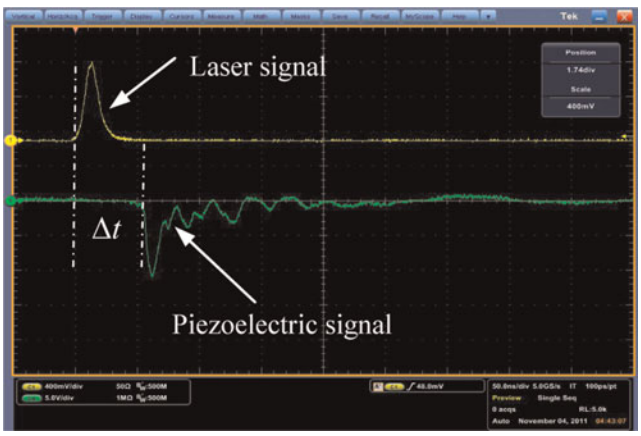


Fig. 9. (Color online) Original signals measured with the photodiode and the piezo film.

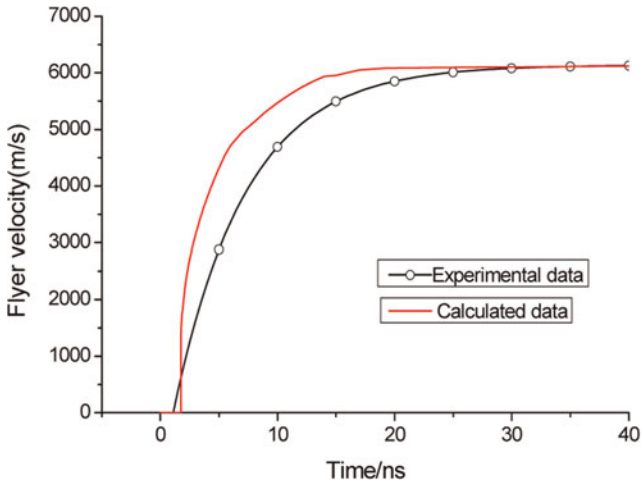


Fig. 10. (Color online) Comparison of computed flyer velocity and experiment data at 300 mJ.

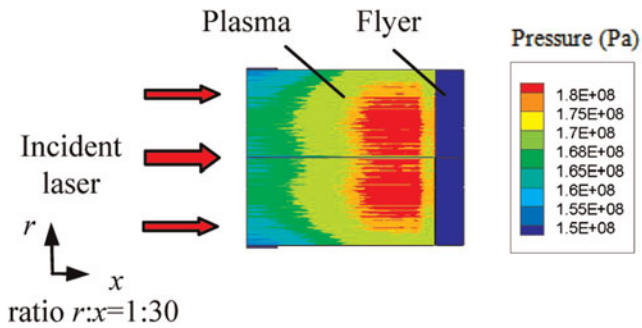


Fig. 11. (Color online) Typical flow field pressure distribution.

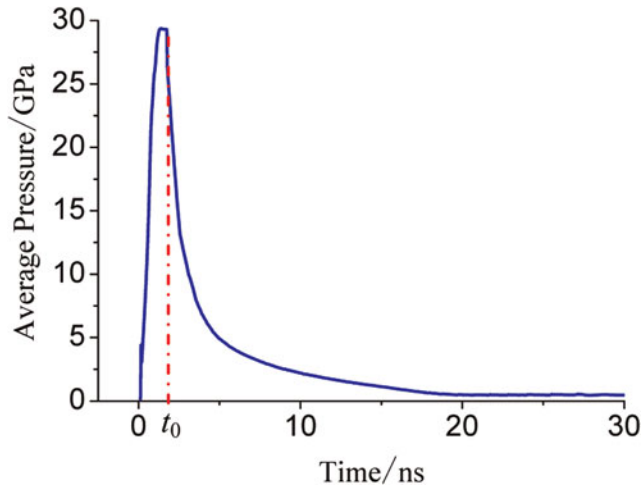


Fig. 12. (Color online) Average pressure of plasma flow field on flyer.

https://doi.org/10.1017/S0263034613000785 Published online by Cambridge University Press

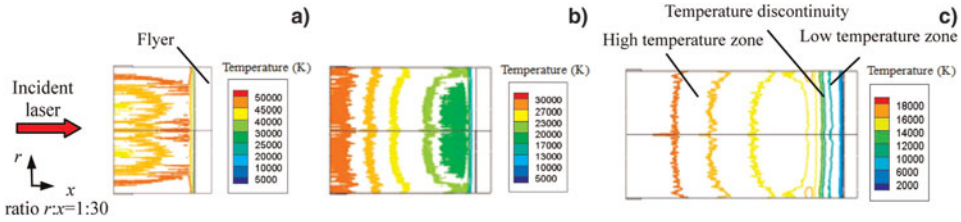


Fig. 13. (Color online) Flow field temperature diagrams at different times. (**a**) 15 ns, (**b**) 22 ns, (**c**) 30 ns.

these experiment data, the double exponential form (Rupp *et al.*, 1999; Paisley *et al.*, 2008) is adopted to describe the flyer plate velocity, then the changing relationship of flyer velocity to time at different laser energies have been obtained (Wang *et al.*, 2012). The confidence is 0.999%.

Comparison of computed flyer velocity and experiment data at laser energy of 300 mJ is plotted in Figure 10. Computed flyer maximum velocity and acceleration time are basically the same as experiment data when resistance coefficient k is 15%. A maximum velocity of 6125 m/s have been reached at about 20 ns. Though flyer velocity at accelerating stage is a little higher than experiment data, the general trend of velocity changes computed essentially agrees with experiment results. Then the value of resistance coefficient k is employed in numerical simulation at other laser energies. Computed flyer maximum velocity and experiment results are listed in Table 3. There were less than 3% error between computation and experiment data.

Plasma Flow Field Analysis

Numerical simulation result at a 300 mJ laser energy is taken for example to analyze plasma flow field changing.

Typical flow field pressure distribution is depicted in Figure 11. Flyer is pushed to move by plasma flow field. As flyer velocity is closely related to the pressure of adjacent flow field, the average pressure of plasma flow field on flyer has been analyzed in Figure 12. For initial stage of laser pulse (2 ns), plasma absorbs laser energy and the average pressure increases gradually before flyer moving. After 2 ns, plasma pressure decreases rapidly as flyer moves and flow field range expands. At 20 ns, the average pressure is basically zero, indicating a maximum velocity for flyer.

Flow field temperature diagrams at different times are presented in Figure 13. It is obvious that at initial stage of laser pulse, flow field temperature decreases gradually along axial direction for less laser energy deposited in film. At 22 ns, temperature distribution is relatively uniform, of around 17000–30000 K. While a temperature discontinuity appears in inner flow field at 30 ns with no laser energy source, dividing the entire flow field into high temperature zone and low temperature zone. The flow field towards laser has a higher temperature, of around 14000–18000 K, and flow field adjacent to flyer has a low temperature of about 2000–10000 K.

Ionized degree is an important parameter to reflect plasma particle composition, relating to flow field temperature and particle number density. Ionized degree distributions of plasma in axial at different times are plotted in Figure 14. Plasma ionization degree at different locations has little difference during laser pulse. Ionization degree increases gradually with laser action time. At 7.5 ns, ionized degree is of around 0.063, while it increases to 0.29 at 15 ns. At 45 ns, laser pulse has already disappeared and a ionized degree discontinuity appears in flow field. The zone adjacent to transparent substrate has a higher ionized degree of 0.43–0.48, indicating more electrical particle, while the flow field near flyer is a low ionized zone with a nearly zero ionized degree, indicating mainly high temperature gas.

Flyer temperature reflects its integrity in some extent. If most of the flyer's temperature far exceeds material vaporization temperature, it may indicates that flyer has already been ablated by plasma and is not intact. Flyer has a good integrity when flyer temperature is much lower for ablating. Compared with single-layered film, insulation layer in multi-layered film can hold back laser energy and prevent flyer from being ablated. In order to clarify the role of insulation layer, temperatures of computed element in axial at 11ns are plotted in Figure 15. Temperature of plasma flow field is of around 42600–42900 K while insulation layer temperature is about 2000 K, flyer temperature basically being 300 K, much lower than its vaporization temperature. It concludes that insulation layer can effectively prevent flyer from being ablated and make sure its integrity.

In laser driven flyer theoretical calculation, Gurney energy theory is normally used to calculate flyer maximum velocity,

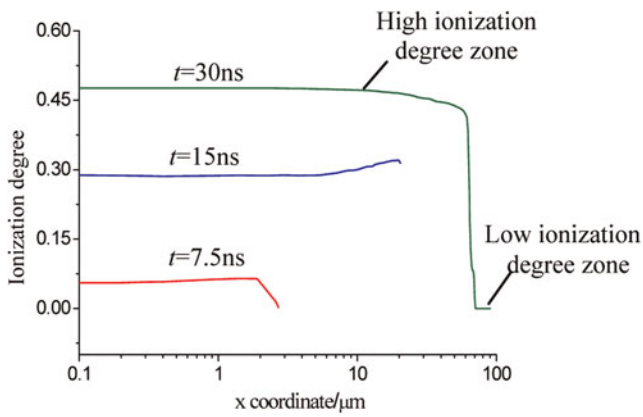


Fig. 14. (Color online) Ionization degree distributions of plasma.

https://doi.org/10.1017/S0263034613000785 Published online by Cambridge University Press

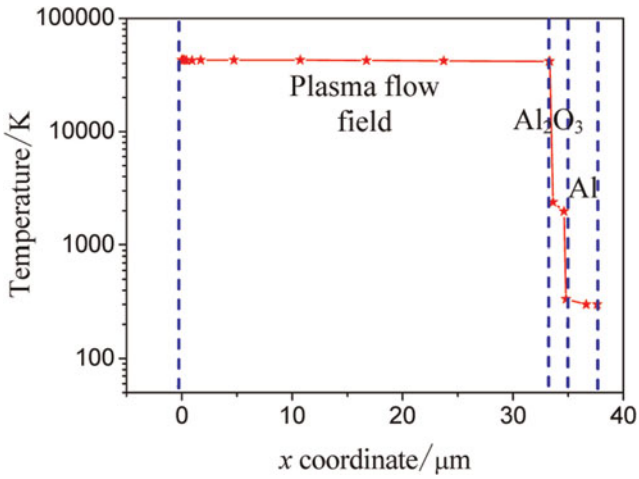


Fig. 15. (Color online) Temperatures of computed elements in axial at different times in axial at 11 ns.

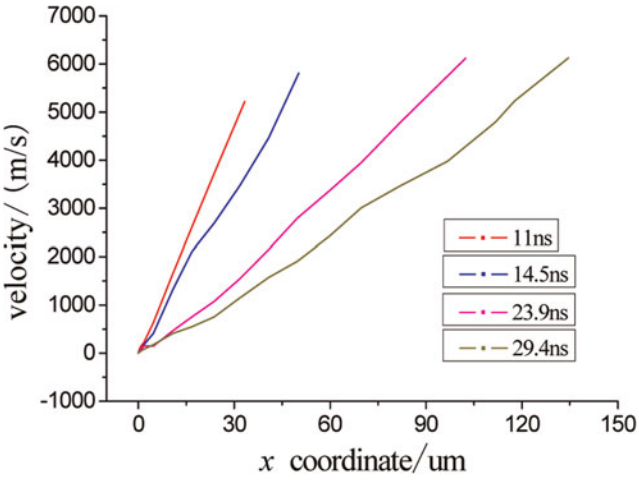


Fig. 16. (Color online) Axial velocity profile of plasma at different times.

with the assumption of plasma velocity increasing from zero to flyer velocity linearly (Lawrence & Trott, 1991). In order to analyze rationality of theoretical assumption, Fig.16 plots plasma axial velocity profile at different times. Computed results show that plasma velocity increases linearly from zero to flyer velocity along flyer motion direction, indicating the rationality of theoretical calculation assumption.

CONCLUSION

Laser energy absorption coefficient should be modified to obtain accurate multi-layered flyer velocity with Gurney energy theory, considering laser energy increase deposited in ablation layer induced by insulation layer. Multi-layered flyer velocity is obviously higher than single-layered flyer at a laser energy density lower than 10 J/cm^2. The difference between multi-layered flyer velocity and single-layered flyer velocity decreases gradually as laser energy density increases. Ablation layer has an optical energy absorption depth for each layer material.

A two-dimensional axisymmetric computation model of laser driven flyer has been established with the consideration of plasma absorption laser energy. Analysis of laser ablation film, plasma formation and flyer motion has been conducted. Numerical simulation of laser driven flyer full process has been achieved. Flyer nearly reaches maximum velocity at the end of laser pulse. Plasma velocity is nearly linear axially during flyer acceleration time. Insulation layer can decreases flyer temperature effectively to keep flyer integrity. Plasma ionization degree distribution is relatively uniform during laser pulse. After laser pulse, ionization degree near transparent substrate is higher, while ionization degree adjacent to flyer is nearly zero, indicating no plasma.

REFERENCES

Bowden, M.D. & Knowles, S.L. (2009). Optimisation of laser-driven flyer velocity using photonic Doppler velocimetry. *SPIE* **7434**, 743403/1–10.

Cazalis, B., Boissière, C. & Sibille, G. (1995). Shocks induced by laser driven flyer plates: 2-Numerical simulations. *AIP* **370**, 1217–1220.

Dai, F., Gong, Z.Z., Cao, Y., Niu, J.C., Tong, J.Y., Xiang, S.M. & Yang, L.M. (2010). Experiment study on technologies for laser-driven flyer hypervelocity launch. *Hi. Power Laser Part. Beams* **22**, 3011–3014.

Damian, C., Johnathan, G.N., Dennis, L.P., Randall, P.J., Sheng, N.L. & Thomas, E.T. (2005). Laser-launched flyer plates for shock physics experiments. *Rev. Sci. Instr.* **76**, 093907/1–9.

Farnworth, A.V. & Lawrence, R.J. (1991). Analytical and computational modeling of small laser-driven flyer plates. Report No. SAND-91-2182C. Washington, DC: Department of Energy.

Gu, Z.W. (2002). Experimental and theoretical research on the high speed flyer driven by laser. PhD Thesis. Mianyang, Sichuang: Chinese Academy of Engineering Physics.

Hong, Y.J., Dou, Z.G., Li, J.M., Yao, H.L. & Luo, J. (2001). The calculating method of equation of state for inert gases. *J. Instit. Command Techn.* **12**, 99–102.

Kadono, T., Yoshida, M., Mitani, N.K., Matsumura, T., Takahashi, E., Matsushima, I., Owadano, Y., Sasatani, Y., Fujita, K., Ozaki, N., Takamatsu, K., Nakano, M., Tanaka, K.A., Takenaka, H., Ito, H. & Kondo, K. (2001). Flyer acceleration experiments using a KrF laser system with a long pulse duration and pressure and thickness of isobaric zone induced in impacted materials. *Laser Part. Beams* **19**, 623–630.

Kazuo, A.T., Motohiko, H., Norimasa, O., Yasufumi, A. & Sergei, I.A. (2000). Multi-layered flyer accelerated by laser induced shock waves. *Phys. Plasma* **7**, 676–680.

Lawrence, R.J. & Trott, W.M. (1991). A simple model for the motion of pulsed-laser-driven thin flyers. *J. Phys. IV.* **1**, 453–458.

Lebo, I.G., Lebo, A.I., Batani, D., Dezulian, R., Benocci, R., Jafer, R. & Krousky, E. (2008). Simulations of shock generation and propagation in laser-plasmas. *Laser Part. Beams* **26**, 179–188.

https://doi.org/10.1017/S0263034613000785 Published online by Cambridge University Press

Moscicki, T., Hoffman, J. & Szymański, Z. (2011). Modeling of plasma formation during nanosecond laser ablation. *Arch. Mechan.* **63**, 99–116.

Paisley, D.L. (1991). Laser-Driven Flyer Plate. Report No. PAT-APPL-7-502956. Washington, DC: Department of Energy.

Paisley, D.L., Luo, S.N.,Greenfield, S.R. & Koskelo, A.C. (2008). Laser-launched flyer plate and confined laser ablation for shock wave loading: Validation and applications. *Rev. Sci. Instr.* **79**, 023902/1–8.

Phipps, C.R., Reilly, J.P. & Campbell, J.W. (2000). Optimum parameters for laser launching objects into low Earth orbit. *Lasers Part. Beams* **18**, 661–695.

Robert, R., Igor, G. & Edvard, G. (2008). Influence of Absorption Mechanisms on Laser-Induced Plasma Plume. *Appl. Surf. Sci.* **254**, 3295–3305.

Rupp, T.D., Gehr, R.J., Harper, R.W., Stahl, D.B., Sheffield, S.A. & Robbins, D.L. (1999). Flyer velocity characteristics of the laser-driven miniflyer system. *Shock Compres. Condensed Matr.* **505**, 1087–1090.

Tong, H.F. & Tang, Z.P. (2008). Simulation of energy coupling of laser and ablated plasma at target surface. *Chinese J. Hi. Pressure Phys.* **22**, 142–148.

Trott, W.M. (1994). Investigation of the dynamic behavior of laser-driven flyers. *Hi. Pressure Sci. Techn.* **309**, 1655–1658.

Wang, F., Chen, L., Wu, J.Y. & Sun, C.Y. (2012). Acceleration characteristics analysis of flyer driven by pulsed laser beam. *Hi. Power Laser Part. Beams* **24**, 2531–2536.

Zeldovich, Y. & Raizer, Y. (1980). *Physics of Shock Waves and High-Temperature Hydrodynamic Phenomena* (Wallace, D.H. & Ronald, F.P., Eds.). New York: Academic Press.

Zhao, X.H., Zhao, X., Shang, G.C. & Gao, Y. (2011). Fiber-coupled laser-driven flyer plates system. *Rev. Aci. Instr.* **82**, 043904/1–8.

https://doi.org/10.1017/S0263034613000785 Published online by Cambridge University Press